

RESEARCH

Open Access



# Development of a generative deep learning model to improve epiretinal membrane detection in fundus photography

Joon Yul Choi<sup>1</sup>, Ik Hee Ryu<sup>2,3</sup>, Jin Kuk Kim<sup>2,3</sup>, In Sik Lee<sup>2</sup> and Tae Keun Yoo<sup>2,3\*</sup>

## Abstract

**Background** The epiretinal membrane (ERM) is a common retinal disorder characterized by abnormal fibrocellular tissue at the vitreomacular interface. Most patients with ERM are asymptomatic at early stages. Therefore, screening for ERM will become increasingly important. Despite the high prevalence of ERM, few deep learning studies have investigated ERM detection in the color fundus photography (CFP) domain. In this study, we built a generative model to enhance ERM detection performance in the CFP.

**Methods** This deep learning study retrospectively collected 302 ERM and 1,250 healthy CFP data points from a healthcare center. The generative model using StyleGAN2 was trained using single-center data. EfficientNetB0 with StyleGAN2-based augmentation was validated using independent internal single-center data and external datasets. We randomly assigned healthcare center data to the development (80%) and internal validation (20%) datasets. Data from two publicly accessible sources were used as external validation datasets.

**Results** StyleGAN2 facilitated realistic CFP synthesis with the characteristic cellophane reflex features of the ERM. The proposed method with StyleGAN2-based augmentation outperformed the typical transfer learning without a generative adversarial network. The proposed model achieved an area under the receiver operating characteristic (AUC) curve of 0.926 for internal validation. AUCs of 0.951 and 0.914 were obtained for the two external validation datasets. Compared with the deep learning model without augmentation, StyleGAN2-based augmentation improved the detection performance and contributed to the focus on the location of the ERM.

**Conclusions** We proposed an ERM detection model by synthesizing realistic CFP images with the pathological features of ERM through generative deep learning. We believe that our deep learning framework will help achieve a more accurate detection of ERM in a limited data setting.

**Keywords** Epiretinal membrane, Fundus photography, Deep learning, Generative adversarial net

## Background

An epiretinal membrane (ERM), also known as an epimacular membrane or macular pucker, is an abnormal semi-translucent film of fibrocellular tissue at the vitreomacular interface (over the internal limiting membrane) [1]. Clinical presentations of ERM include: decreased visual acuity, metamorphopsia, micropsia, and monocular diplopia. However, most patients with ERM are asymptomatic at early stages. The prevalence of ERM

\*Correspondence:

Tae Keun Yoo

[eyetaekeyunoo@gmail.com](mailto:eyetaekeyunoo@gmail.com); [fawoo2@yonsei.ac.kr](mailto:fawoo2@yonsei.ac.kr)

<sup>1</sup> Department of Biomedical Engineering, Yonsei University, Wonju, South Korea

<sup>2</sup> Department of Refractive Surgery, B&VIT Eye Center, B2 GT Tower, 1317-23 Seocho-Dong, Seocho-Gu, Seoul, South Korea

<sup>3</sup> Research and development department, VISUWORKS, Seoul, South Korea



© The Author(s) 2024. **Open Access** This article is licensed under a Creative Commons Attribution 4.0 International License, which permits use, sharing, adaptation, distribution and reproduction in any medium or format, as long as you give appropriate credit to the original author(s) and the source, provide a link to the Creative Commons licence, and indicate if changes were made. The images or other third party material in this article are included in the article's Creative Commons licence, unless indicated otherwise in a credit line to the material. If material is not included in the article's Creative Commons licence and your intended use is not permitted by statutory regulation or exceeds the permitted use, you will need to obtain permission directly from the copyright holder. To view a copy of this licence, visit <http://creativecommons.org/licenses/by/4.0/>. The Creative Commons Public Domain Dedication waiver (<http://creativecommons.org/publicdomain/zero/1.0/>) applies to the data made available in this article, unless otherwise stated in a credit line to the data.

generally increases with age. According to a previous report, 30 million adults in the United States have ERM. In a nationwide study in South Korea, the prevalence of ERM was reported as 2.9–7.0% [2, 3]. The prevalence rate is expected to increase in aging societies. ERM can be treated by vitreoretinal surgery using a pars plana vitrectomy procedure and membrane peeling [4]. If the fibrocellular tissue is detected early and removed by surgery before vision decreases, vision loss can be prevented. Most ERMs have no specific causes. Therefore, screening for ERM will become increasingly important.

Recently, the detection of ERM using optical coherence tomography (OCT) was established [1]. OCT reveals a hyperreflective layer of the fibrocellular membrane tissue by directly imaging the vitreoretinal interface. However, OCT is unsuitable as a retinal screening method because of its relatively long measurement time and difficulty in configuring the equipment. ERM can be diagnosed based on fundus examination or color fundus photography (CFP), as shown in Fig. 1. The cellophane reflex in the macular area can be observed by careful examination of eyes with ERM [5]. There can be an irregular foveal

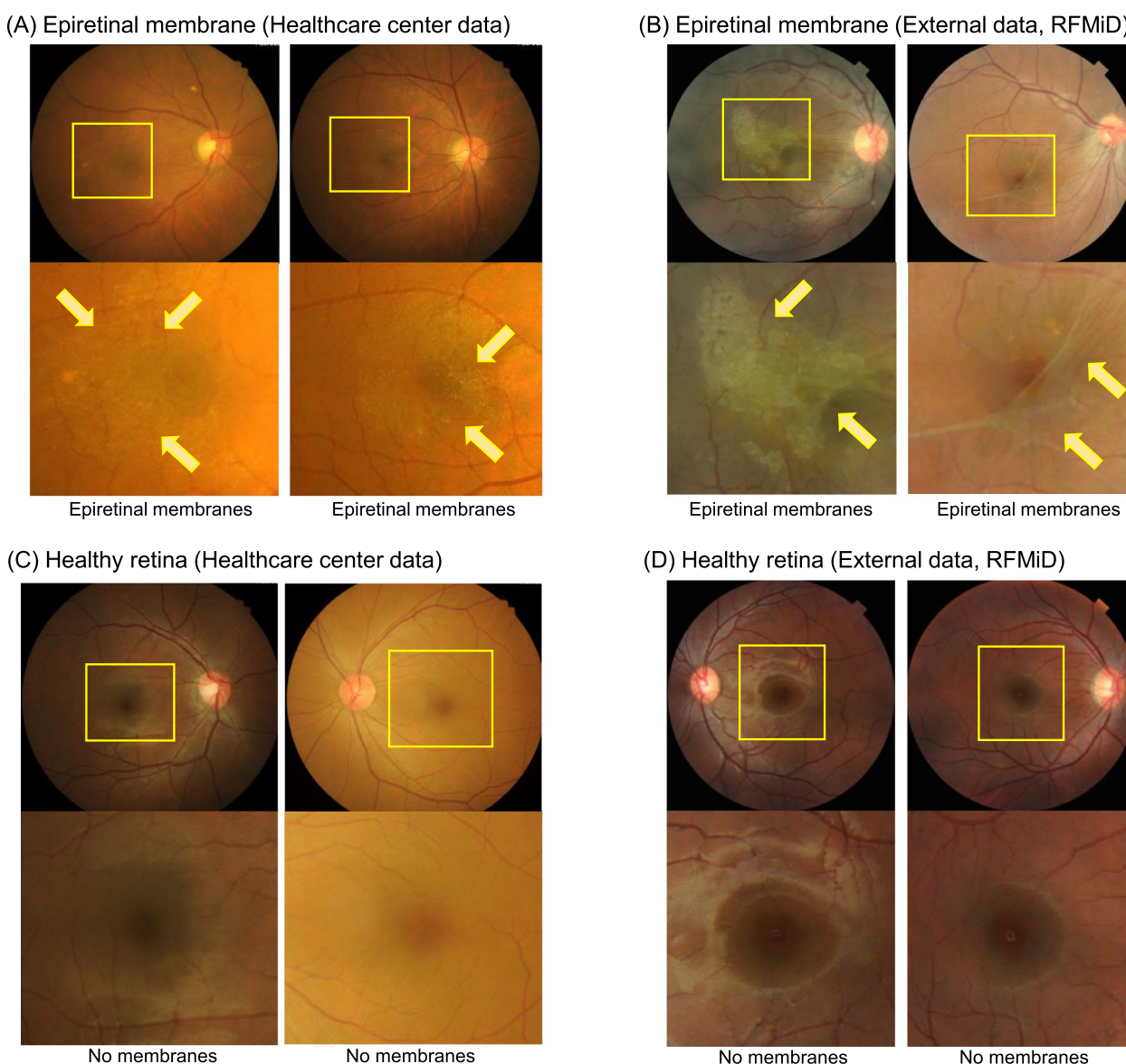


**Fig. 1** Representative fundus photographs (FPs) of the abnormal semi-translucent film of fibro-cellular tissues of epiretinal membranes (ERM) with reduced visual acuity and healthy retinas. **A** FP with ERM from the healthcare center data. **B** FP with ERM from the external validation data. **C** FP with healthy retina from the healthcare center data. **D** FP with healthy retina from the external validation data

contour or a wrinkled retinal surface due to contracture of the fibrocellular membrane. However, because the membrane tissue is transparent, it is possible to misdiagnose ERM using fundus photographs. Most studies using artificial intelligence (AI) to diagnose ERM have concentrated in the OCT image domain [6, 7].

Considering the high prevalence of ERM, few AI-based studies have attempted to investigate ERM detection in the CFP domain compared to many other studies on diabetic retinopathy, age-related macular degeneration, and glaucoma [8, 9]. A previous study focused on the diagnosis of ERM through CFP using deep learning; however, the accuracy was relatively low [10]. This low accuracy was attributed to the relative lack of CFP data with ERM. Several previous studies on a big-data scale have analyzed ERM as a subclass for multiclass retinal disease classification [11–13]. Recently, generative artificial intelligence (AI) was introduced to overcome the lack of data on rare diseases [14]. In this study, we synthesized CFP images with ERM by using a generative AI technique (generative adversarial network; GAN). Using the augmented data generated by StyleGAN2, we improved the diagnostic accuracy of the deep learning models for detecting ERM (Fig. 2). To confirm the performance, we validate the models using external datasets.

**Methods**

**Data collection**

We retrospectively collected CFP data containing ERM from an Eye Care Center (B&VIIT Eye Center, Seoul,

South Korea). This study was approved by the Institutional Review Board of the Korean National Institute for Bioethics Policy (KNIBP) and the requirement for informed consent was waived. All procedures were performed in accordance with the ethical standards of the institutional and national research committees and the 1964 Declaration of Helsinki and its later amendments or comparable ethical standards. The clinical data of human participants, except for CFP, were not obtained in this study. We collected CFP images from patients with ERM diagnosed with the KCD code H3539 (ICD-10 code H35.379) between January 2015 and December 2022. External validation was conducted using publicly accessible CFP databases to validate the developed deep learning models. The external databases include: the retinal fundus multi-disease image dataset (RFMiD) [15] and the Joint Shantou International Eye Center dataset (JSIEC) [12].

Data processing is demonstrated in the Supplementary Materials. The healthcare center dataset consisted of CFP images of 1,250 healthy eyes and 302 eyes with ERM. The training and internal validation datasets were obtained using healthcare center data and were randomly split. We assigned 1,239 CFP images (80%, including 1000 healthy and 239 ERM) to the training dataset, and 313 images (20%, including 250 healthy and 63 ERM) were used as the internal validation dataset. The GAN-based method augments ER images with proper diversity and high quality to improve diagnostic performance. After augmenting the training data for ERM, we trained deep learning

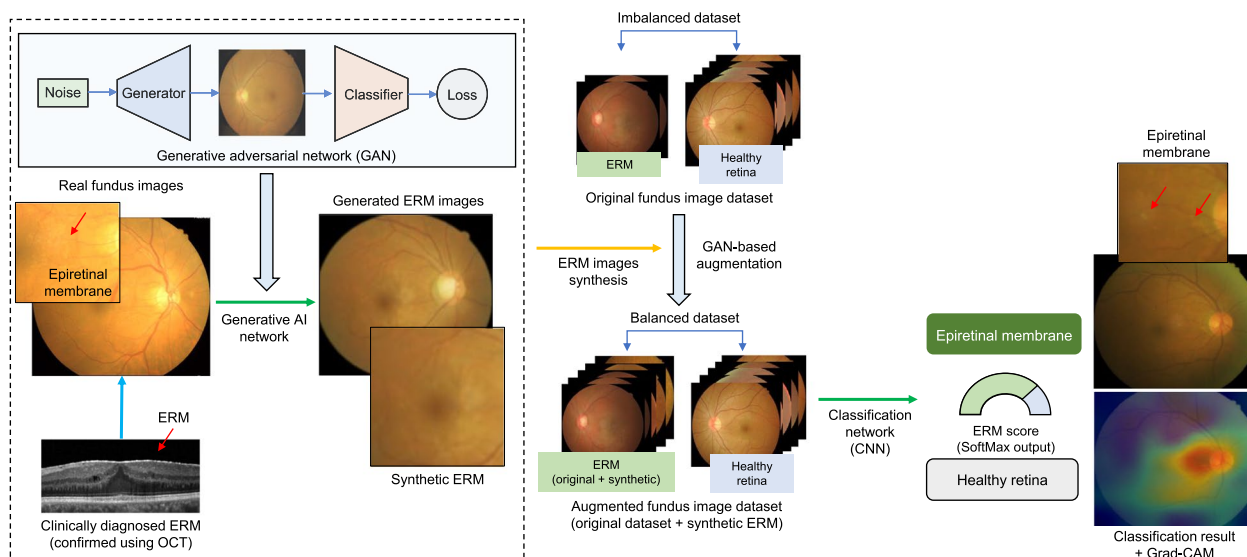


**Fig. 2** Schematic diagram of the development of deep learning model for epiretinal membrane (ERM) detection. The generative adversarial network (GAN) model augments ERM images with proper diversity and high quality to improve diagnostic performance. After augmenting the training data for ERM, we trained deep learning networks via transfer learning to classify ERM and healthy retinas

networks via transfer learning to classify ERM separately from healthy retinas. Two external validation procedures were performed. We collected the RFMiD test set (669 healthy retinas and 26 ERM) and JSIEC dataset (38 healthy retinas and 26 ERM). The labels on the datasets from the healthcare center and publicly accessible sources were confirmed by an ophthalmologist. The data flow is shown in Fig. 3. We confirmed that the training of the GAN and convolutional neural network (CNN) models were performed using only the training dataset and that there was no overlap in the training (for both the GAN and CNN) and validation datasets, as shown in Fig. 3.

### GAN image synthesis

With recent vigorous research on generative AI, GAN has been established as a standard method for generating medical images [16]. As the GAN model learns the image pixel data distribution for data synthesis, the training dataset requires a sufficient volume to train the generator without mode collapse or overfitting. We attempted to overcome this problem of overfitting using traditional augmentation techniques with simple geometric transformations. Traditional data augmentation was performed using linear spatial transformation including: left and right flipping, width/height translation from

-5% to +5%, random rotation from -15° to 15°, zooming from 0 to 15%, and random brightness change from -10% to 10%. Initially, we prepared 4000 healthy and 1000 ERM CFP images to train the GAN. As shown in Fig. 3, we attempted to improve the performance of the deep-learning classifiers by creating an additional 2000 synthetic CFPs with ERM using the GAN algorithm. It aims to eliminate data imbalance and further generalize the model by supplementing more diverse and realistic synthetic data through the GAN.

In this study, we adopted the deep convolutional GAN (DCGAN), CycleGAN, and StyleGAN2, which are the most popular GAN techniques in the medical field [17]. The DCGAN is a basic form of GAN architecture based on the vanilla GAN that replaces the building block of the generator with fully convolutional layers [18]. DCGAN has been successfully used to synthesize CFP images of glaucoma [19]. CycleGAN is the most popular unpaired image-to-image translation GAN technique [14]. The basic concept of CycleGAN is cyclic consistency, in which the training algorithm matches the features of the image data distribution between two classes in an unpaired dataset. CycleGAN was used to generate denoised CFP images from images with artifacts [20]. Recently, StyleGAN2 has been well-adopted to synthesize high-resolution images [21, 22]. StyleGAN employs

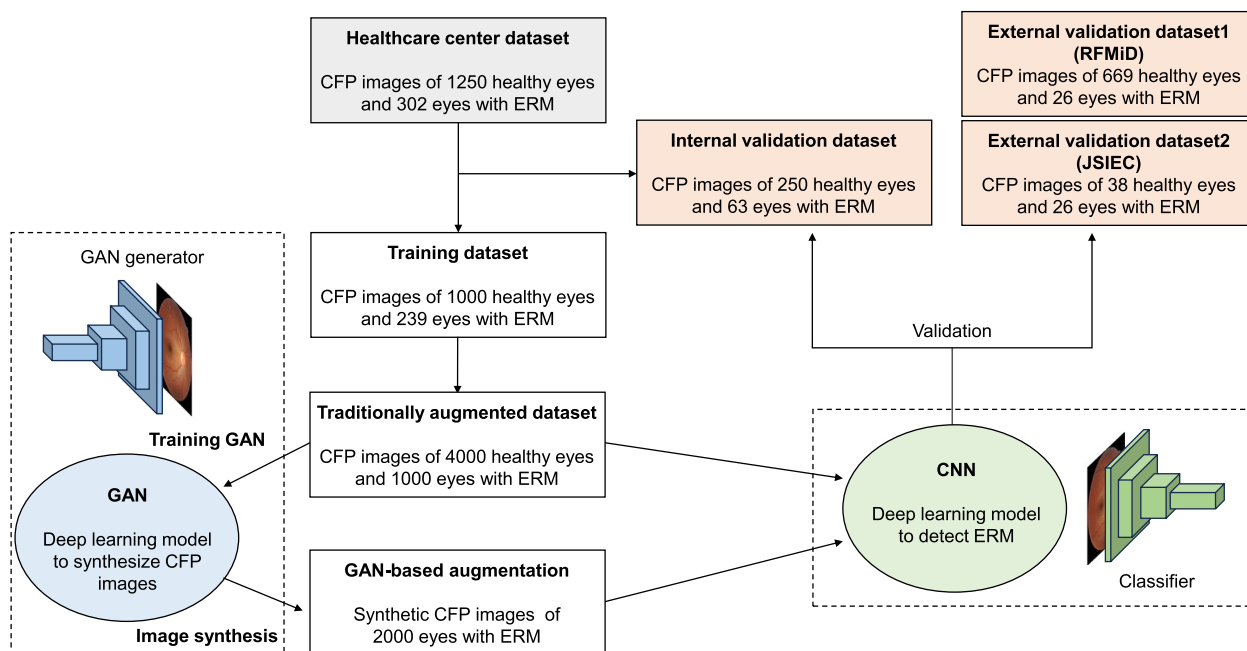


**Fig. 3** Dataset used in developing and validating the epiretinal membrane detection model in fundus photography. The deep learning models were trained and internally validated using randomly partitioned 80 and 20% of data, respectively. Using the training dataset, GAN models were trained to increase the volume of the ERM dataset for data augmentation. We finally built an ERM detection model based on the GAN augmentation techniques. The two external validation datasets, including RFMiD and JSIEC, represented a real scenario of a check-up center with CFP screening

the concepts of similarity and aversion. StyleGAN demonstrated good performance in synthesizing high-resolution CFP images [23]. StyleGAN2, which is an advanced version of StyleGAN, has been successfully adopted in the medical field for knee radiography and colonoscopy image synthesis [17, 24]. The sources of the backbone codes of the GAN architectures are shown in the Supplementary Materials section and were modified to adapt to CFP synthesis. The size of the output images was set to a resolution of  $256 \times 256$  pixels to use the default architecture of the GAN models. The GAN models were trained using the same dataset. In our experience, owing to the limitations of the volume of data, the GAN model did not properly learn using only with CFP images of ERM. Therefore, the healthy retina data were learned together with the ERM to properly generate realistic CFP images. DCGAN and StyleGAN2 were trained by combining both healthy retinas and ERM data, and the generated ERM data were used for further deep-learning training. By contrast, CycleGAN separates healthy and ERM data to learn domain translation and generates ERM data by infusing pathological characteristics into healthy images. An ophthalmologist reviewed the CFP images generated by the GAN models and removed the synthetic images with artifacts or without ERM features. Only generated images that confirmed the structures of the optic disc and vascular arcades classical of ERM were used for training. This manual selection process was performed to improve the diagnostic performance of GAN-based augmentation. Finally, we generated 2,000 synthetic CFP images with ERM for each GAN technique to train the CNN models. The deep-learning models were trained using an NVIDIA RTX 2080Ti GPU with 4,352 CUDA cores and 11 GB of RAM.

### CNN model training

After the GAN-based augmentation to enrich the ERM data, we built a CNN classifier model for ERM detection. We used ResNet50 and EfficientNetB0 as the backbone CNN models for the classifiers. These architectures have been recognized as standard models owing to their robustness and performance [25]. The CNN architectures were pre-trained on general image features from the ImageNet data and imported into the workspace. The input images were resized to the input tensor of each original CNN architecture ( $224 \text{ pixels} \times 224 \text{ pixels}$  for ResNet50 and EfficientNetB0). The last layers of the CNN architecture were replaced with a modified fully connected network layer (with  $2 \times 2048$  weights and  $2 \times 1$  bias) and two softmax functions for the two classes (ERM and healthy), which set the output of the prediction score to a range of zero to one, which corresponds to the prediction probability of each class. All CNN training procedures were

optimized using stochastic gradient descent (SGD) with a momentum algorithm (SGD learning rate = 0.0001) and a mini-batch size of 20 over 100 epochs, which are the fine-tuning parameters for transfer learning. Using the Grad-CAM technique, attention heat maps were generated from the last layers of the softmax and the activation convolutional layers of the trained CNN model. This visualization indicates whether the CNN model was properly trained with a focus on the ERM features. To determine the best data-augmentation strategy, we trained the CNN weights using no augmentation, simple geometric transformation (classic augmentation) to balance the case-control datasets (ERM data oversampling), and GAN-based augmentation. For an additional comparison experiment, we adapted the denoising diffusion probabilistic model (DDPM) [26, 27] and CutMix [28] to augment the ERM data. A pretrained vision transformer (ViT) with transfer learning software [29] was used to check whether the performance could be improved.

### Statistical analysis

The performance of the CNN models for detecting ERM was evaluated using metrics including: the area under the curve (AUC) of the receiver operating characteristics (ROC), sensitivity, and specificity. Due to the characteristics of the imbalanced data, we adopted Youden's index, a standard threshold method that assigns equal weights to sensitivity and specificity.

### Results

Initially, we trained the GAN models based on traditional augmentation. Figure 4 shows the representative results of GAN image generation. The CFP images with ERM synthesized showed the basic structures of the macula, with the optic nerve, vascular arcade, and fovea, for all GAN techniques. The synthetic images generated by the DCGAN were of low quality and had distinct artifacts. The synthetic images generated by the CycleGAN also had some checkerboard artifacts and showed insignificant ERM features. Compared to DCGAN and CycleGAN, StyleGAN2 synthesizes realistic CFP images with significant ERM features. After an ophthalmologist reviewed the images generated by the GAN models, we retained 2,000 CFP images with ERM for each GAN technique and added them to the original training dataset. As shown in Fig. 5, an ERM attribute can be infused into the CFP by adjusting the latent space of the trained StyleGAN2 in a certain direction. However, because ERM is not completely independent of other factors, other changes in CFP are associated with ERM generation.

Figure 6 shows the ROC curves for the ERM detection results of the EfficientNetB0 models for the internal and external validation results. Table 1 shows the ERM

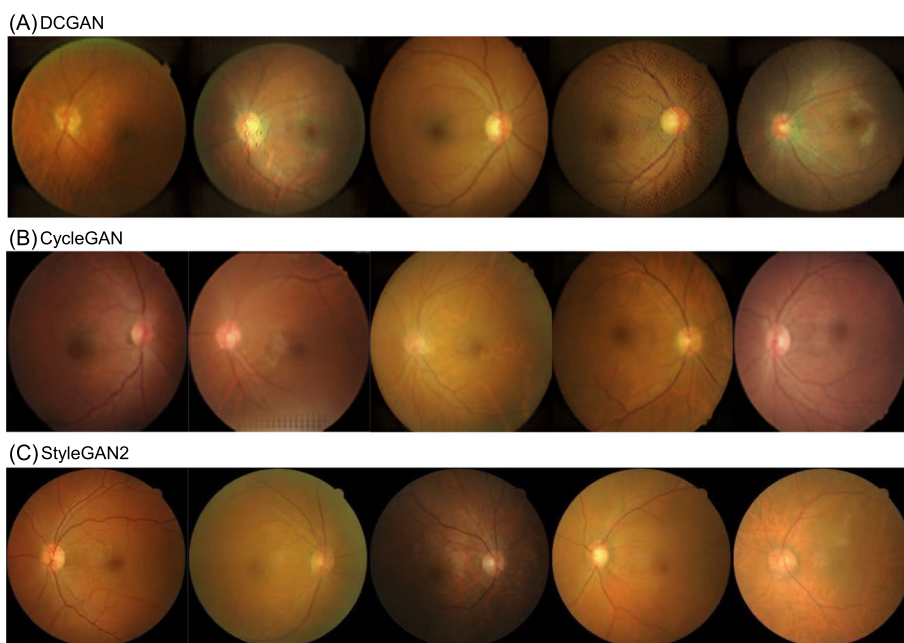


**Fig. 4** Epiretinal membrane image generation using generative AI algorithms. **A** DCGAN. **B** CycleGAN. **C** StyleGAN2

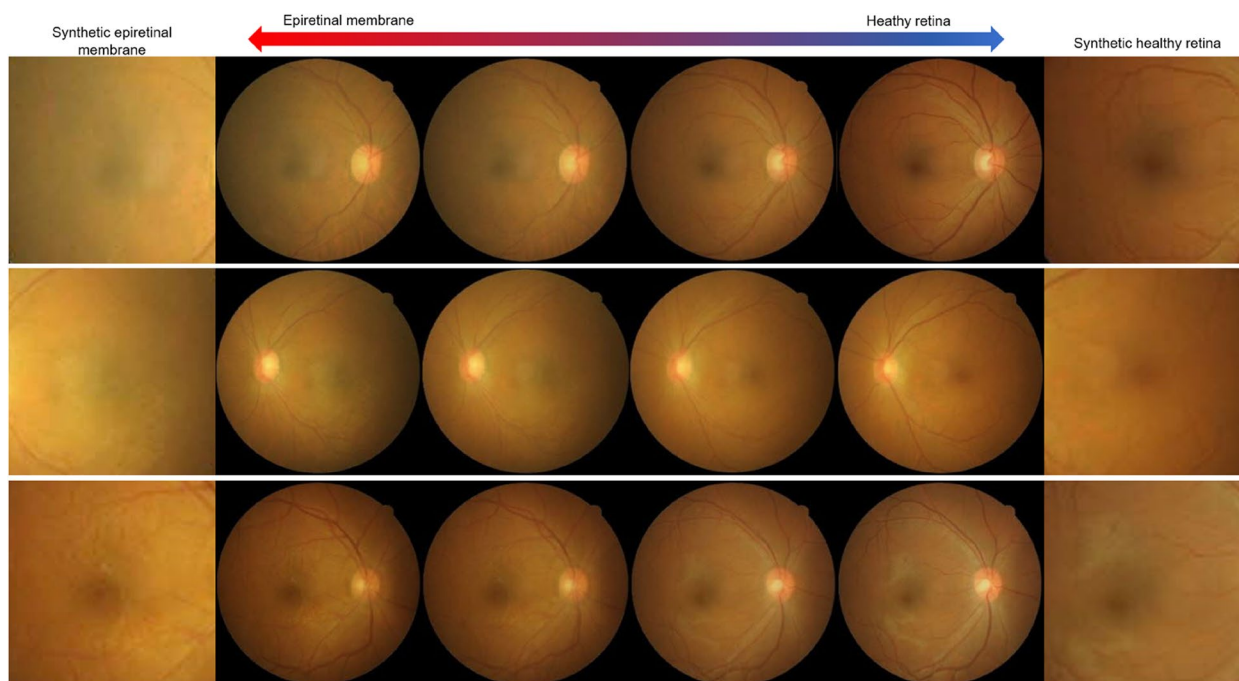


**Fig. 5** Synthetic fundus photographs according to latent space changes in the StyleGAN2 model

detection performance using the internal validation dataset. EfficientNetB0 trained with StyleGAN2 augmentation exhibited the best detection performance. The AUC of the proposed styleGAN2 method was 0.926 (95% confidence interval [CI], 0.890–0.963), which was better than that of the

other models. It yielded a sensitivity of 92.0% (95% CI, 82.4–97.3%), a specificity of 80.8% (95% CI, 75.3–85.4%), a PPV of 54.7% (95% CI, 48.1–61.1), and an NPV of 97.5% (95% CI, 94.5–98.9%). In both ResNet50 and EfficientNetB0 architectures, augmentation with StyleGAN2 resulted in better

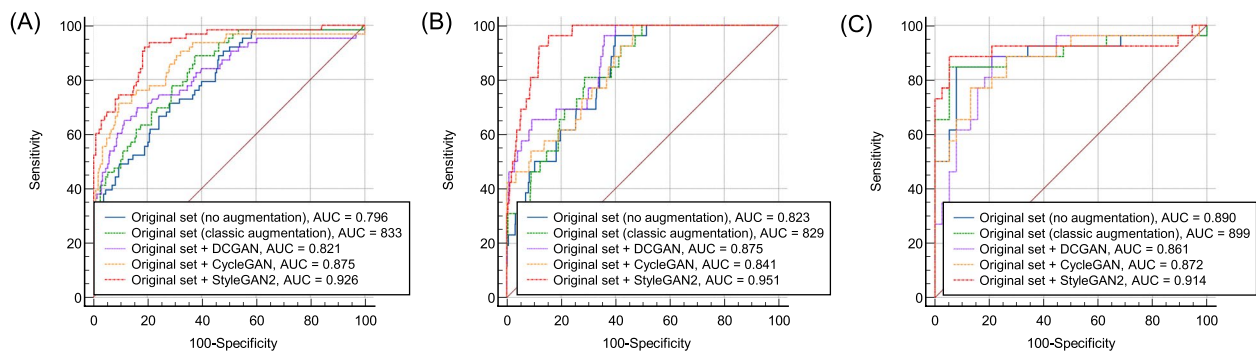


**Fig. 6** Validation results of ROC curves for detection of epiretinal membrane. **A** Healthcare center dataset. **B** External dataset 1 (RFMiD). **C** External dataset 2 (JSIEC)

**Table 1** The prediction results from the internal validation (healthcare center dataset) to detect epiretinal membrane in fundus photographs

CNN architectures	Training set	ROC-AUC (95% CI)	Sensitivity (% , 95% CI)	Specificity (% , 95% CI)	PPV (% , 95% CI)	NPV (% , 95% CI)
ResNet50	Original set (no augmentation)	0.766 (0.702–0.830)	71.4 (58.6–82.1)	70.4 (64.3–75.9)	37.8 (32.2–43.7)	90.7 (86.7–93.6)
	Original set + classic augmentation <sup>a</sup>	0.827 (0.780–0.867)	92.1 (82.4–97.4)	58.0 (51.6–64.2)	35.6 (31.9–39.4)	96.7 (92.5–98.5)
	Original set + DCGAN	0.850 (0.798–0.902)	90.4 (80.4–96.4)	63.6 (57.3–69.5)	38.5 (34.2–42.9)	96.3 (92.4–98.2)
	Original set + CycleGAN	0.859 (0.803–0.914)	79.3 (67.3–88.5)	78.8 (73.2–83.6)	48.5 (41.8–55.2)	93.8 (90.2–96.1)
	Original set + StyleGAN2	0.913 (0.872–0.954)	90.4 (80.4–96.4)	75.6 (69.7–80.7)	48.3 (42.5–54.1)	96.9 (93.6–98.5)
EfficientNetB0	Original set (no augmentation)	0.796 (0.736–0.855)	71.4 (58.6–82.1)	71.6 (65.5–77.1)	38.7 (33.0–44.8)	90.8 (86.9–93.6)
	Original set + classic augmentation <sup>a</sup>	0.833 (0.786–0.872)	88.9 (78.4–95.4)	62.4 (56.1–68.4)	37.3 (33.2–41.6)	95.7 (91.7–97.8)
	Original set + DCGAN	0.821 (0.756–0.887)	65.0 (52.0–76.6)	88.4 (83.7–92.0)	58.5 (48.9–67.5)	90.9 (87.7–93.3)
	Original set + CycleGAN	0.875 (0.821–0.929)	71.4 (58.6–82.1)	90.4 (86.0–93.7)	65.2 (55.4–73.8)	92.6 (89.4–94.8)
	Original set + StyleGAN2	0.926 (0.890–0.963)	92.0 (82.4–97.3)	80.8 (75.3–85.4)	54.7 (48.1–61.1)	97.5 (94.5–98.9)

CI confidence interval, NPV negative predictive value, PPV positive predictive value, ROC-AUC area under the receiver operating characteristic curve

<sup>a</sup> We oversample the ERM class to balance the training dataset

AUCs than the other GAN techniques. The deep learning models with classic linear augmentation were inferior to EfficientNetB0 trained with StyleGAN2 augmentation.

The external validation results obtained using the RFMiD dataset are listed in Table 2. The EfficientNetB0 trained with StyleGAN2 augmentation also showed the highest AUC- 0.951 (95% CI, 0.926–0.976)-among the developed models. This model detected crystalline retinopathy with a sensitivity of 96.1% (95% CI, 80.3–99.9%), a specificity of 85.6% (95% CI, 81.6–87.2%), a PPV of 19.5% (95% CI, 16.6–22.7%), and an NPV of 99.8% (95% CI, 98.8–99.9%). Similar results were observed for other external validations using the JSIEC dataset (Table 3). EfficientNetB0 trained with StyleGAN2 augmentation also showed a detection performance with an AUC of 0.914 (95% CI, 0.818–0.999). The corresponding sensitivity, specificity, PPV, and NPV were 88.4% (95% CI, 69.8–97.5%), 94.7% (95% CI, 82.2–99.3%), 92.0% (95% CI, 74.7–97.8%), and 92.3 (95% CI, 80.5–97.2%), respectively.

To further determine whether the models properly analyzed the ERM features of the CFP, we generated attention maps of the EfficientNetB0 models using the Grad-CAM technique (Fig. 7). Using EfficientNetB0 trained with StyleGAN2 augmentation, Grad-CAM frequently focused on the central area of the macula and visualized the characteristic pathological features of ERM (cellophane reflex). EfficientNetB0, trained without GAN augmentation, frequently highlighted peripheral areas of the macula or margins of the ERM that did not match the exact location of the ERM.

Table 4 presents a comparison between the proposed method (EfficientNetB0 trained with StyleGAN2 augmentation) and recent deep learning techniques. ERM data augmentation based on the DDPM and CutMix failed to achieve a performance comparable to that of the proposed model ( $P < 0.050$ ). The ViT model with classic data augmentation also exhibited a lower ROC AUC than the proposed model. The difference between the

**Table 2** The prediction results from an external validation dataset (RFMiD) to detect epiretinal membrane in fundus photographs

CNN architectures	Training set	ROC-AUC (95% CI)	Sensitivity (%; 95% CI)	Specificity (%; 95% CI)	PPV (%; 95% CI)	NPV (%; 95% CI)
ResNet50	Original set (no augmentation)	0.873 (0.806–0.941)	65.3 (44.3–82.7)	90.4 (87.9–92.5)	20.9 (15.5–27.6)	98.5 (97.5–99.1)
	Original set + classic augmentation <sup>a</sup>	0.849 (0.820–0.875)	88.5 (69.8–97.5)	69.5 (65.8–72.9)	10.1 (8.6–11.9)	99.4 (98.1–99.8)
	Original set + DCGAN	0.914 (0.869–0.959)	88.4 (69.8–97.5)	76.8 (73.4–79.9)	12.9 (10.8–15.2)	99.4 (98.3–99.7)
	Original set + CycleGAN	0.863 (0.811–0.914)	80.7 (60.6–93.4)	79.8 (76.5–82.8)	13.4 (10.8–16.5)	99.0 (97.9–99.5)
	Original set + StyleGAN2	0.939 (0.899–0.979)	84.6 (65.1–95.6)	88.3 (85.6–90.6)	22.0 (17.8–26.8)	99.3 (98.3–99.7)
EfficientNetB0	Original set (no augmentation)	0.823 (0.759–0.886)	96.1 (80.3–99.9)	60.0 (56.2–63.8)	8.5 (7.6–9.5)	99.7 (98.3–99.9)
	Original set + classic augmentation <sup>a</sup>	0.829 (0.799–0.857)	80.8 (60.6–93.4)	70.4 (66.8–73.8)	9.6 (7.8–11.7)	98.9 (97.7–99.5)
	Original set + DCGAN	0.875 (0.815–0.935)	96.1 (80.3–99.9)	64.1 (60.3–67.7)	9.4 (8.4–10.5)	99.7 (98.4–99.9)
	Original set + CycleGAN	0.841 (0.773–0.908)	100 (86.7–100)	53.5 (49.6–57.3)	7.7 (7.1–8.3)	100 (98.9–100)
	Original set + StyleGAN2	0.951 (0.926–0.976)	96.1 (80.3–99.9)	84.6 (81.6–87.2)	19.5 (16.6–22.7)	99.8 (98.8–99.9)

CI confidence interval, NPV negative predictive value, PPV positive predictive value, RFMiD Retinal fundus multi-disease image dataset, ROC-AUC area under the receiver operating characteristic curve

<sup>a</sup> We oversampled the ERM class to balance the training dataset

**Table 3** The prediction results from the external validation dataset (JSIEC) to detect epiretinal membrane in fundus photographs

CNN architectures	Training set	ROC-AUC (95% CI)	Sensitivity (%; 95% CI)	Specificity (%; 95% CI)	PPV (%; 95% CI)	NPV (%; 95% CI)
ResNet50	Original set (no augmentation)	0.808 (0.703–0.912)	88.4 (69.8–97.5)	60.5 (43.3–75.9)	60.5 (50.2–69.9)	88.4 (71.9–95.8)
	Original set + classic augmentation <sup>a</sup>	0.849 (0.738–0.926)	92.3 (74.9–99.1)	71.1 (54.1–84.6)	68.6 (56.7–78.4)	93.1 (77.8–98.1)
	Original set + DCGAN	0.866 (0.753–0.980)	92.3 (74.8–99.0)	76.3 (59.7–88.5)	72.7 (59.8–82.6)	93.5 (79.0–98.2)
	Original set + CycleGAN	0.879 (0.796–0.961)	69.2 (48.2–85.6)	89.4 (75.1–97.0)	81.8 (63.2–92.1)	80.9 (70.2–88.4)
	Original set + StyleGAN2	0.910 (0.817–0.983)	76.9 (56.3–91.0)	92.1 (78.6–98.3)	86.9 (68.8–95.2)	85.3 (74.1–92.2)
EfficientNetB0	Original set (no augmentation)	0.890 (0.794–0.985)	84.6 (65.1–95.6)	92.1 (78.6–98.3)	88.0 (70.9–95.6)	89.7 (77.9–95.5)
	Original set + classic augmentation <sup>a</sup>	0.899 (0.798–0.960)	84.6 (65.1–95.6)	94.7 (82.3–99.4)	91.7 (73.9–97.7)	90.0 (78.5–95.7)
	Original set + DCGAN	0.861 (0.764–0.959)	92.3 (74.8–99.0)	76.3 (59.7–88.5)	72.7 (59.8–82.6)	93.5 (79.0–98.2)
	Original set + CycleGAN	0.871 (0.778–0.967)	76.9 (56.3–91.0)	86.8 (71.9–95.5)	80.0 (63.2–90.2)	84.6 (72.9–91.8)
	Original set + StyleGAN2	0.914 (0.818–0.999)	88.4 (69.8–97.5)	94.7 (82.2–99.3)	92.0 (74.7–97.8)	92.3 (80.5–97.2)

CI confidence interval, JSIEC Joint Shantou International Eye Center, NPV negative predictive value, PPV positive predictive value, ROC-AUC area under the receiver operating characteristic curve

<sup>a</sup> We oversampled the ERM class to balance the training dataset

proposed model and the ViT trained with StyleGAN2 augmentation was not significant ( $P=0.0914$ ).

## Discussion

We aimed to synthesize CFPs with ERM using GAN techniques to address the data imbalance problem. We built an improved ERM detection model using StyleGAN2-based augmentation. Previous studies have focused on detecting ERM in CFP images using deep learning [10, 31]. However, the clinical application of the previous models was difficult because the ability to detect ERM was relatively low, and there was no external validation. Compared with previous studies, our approach additionally boosts the ERM detection performance by synthesizing CFP images using StyleGAN2, which combines normal and pathological CFPs to generate realistic

synthetic images. Our study demonstrates that generative AI techniques can be used to address the lack of medical data in the CFP image domain.

Grad-CAM heatmaps showed that the proposed classification model properly analyzed the ERM features. Compared with the CNN model without augmentation, the StyleGAN2-based augmentation process focused on the location of the ERM. If a small number of training sets is used, the risk of overfitting always exists, and it is expected that the StyleGAN2 has helped to avoid overfitting. Based on this technique, our study achieved a better performance (0.926 of AUC) than that of a previous study (0.857 of AUC) in detecting ERM [10]. Several studies have developed deep learning models to detect ERM [12, 13]; however, the validation sets were different, and additional studies are needed to compare the objective performance of various deep learning models to detect ERM.



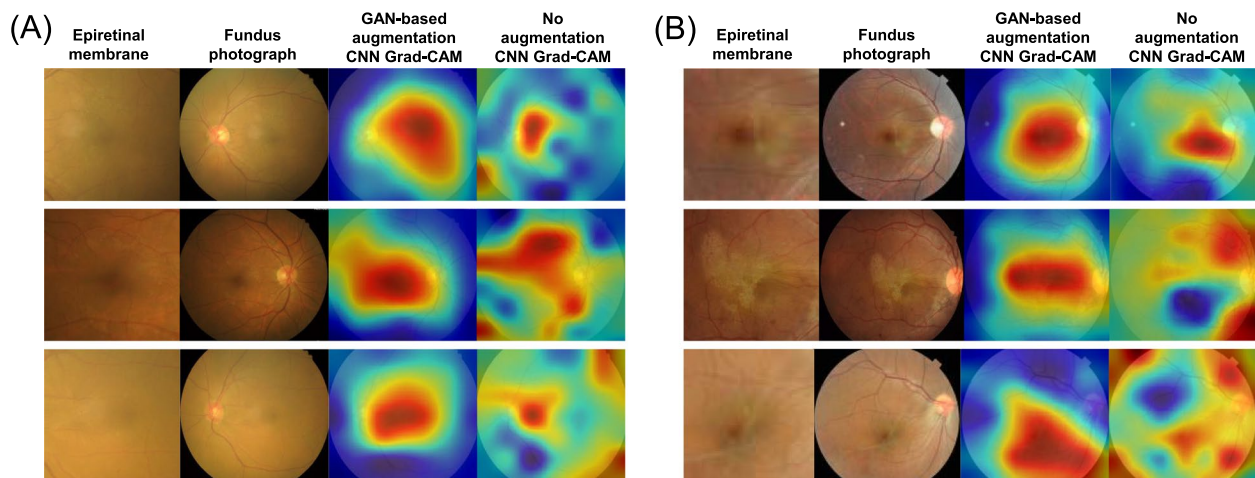


**Fig. 7** Attention maps generated by the Grad-CAM technique from the developed EfficientNetB0 to detect epiretinal membrane. **A** Healthcare center dataset. **B** External dataset (RFMiD)

**Table 4** Comparison of prediction performance from internal validation (healthcare center dataset) to detect epiretinal membrane in fundus photographs

Classification network architecture	Augmentation	ROC-AUC (95% CI)	Sensitivity (% , 95% CI)	Specificity (% , 95% CI)	P-value
EfficientNetB0	StyleGAN2 (Ours)	0.926 (0.890–0.963)	92.0 (82.4–97.3)	80.8 (75.3–85.4)	Reference
EfficientNetB0	DDPM [26, 27]	0.825 (0.779–0.866)	88.9 (78.4–95.4)	65.2 (58.9–71.1)	0.0048
EfficientNetB0	CutMix <sup>a</sup> [28]	0.837 (0.792–0.877)	77.8 (65.5–87.3)	86.0 (81.1–90.1)	0.0080
Vision Transformer [29]	Classic augmentation <sup>a</sup>	0.835 (0.789–0.874)	84.1 (72.7–92.1)	75.2 (69.4–80.4)	0.0051
Vision Transformer [29]	StyleGAN2	0.863 (0.819–0.899)	82.5 (70.9–90.9)	84.0 (78.9–88.3)	0.0914

CI confidence interval, DDPM denoising diffusion probabilistic model, ROC-AUC area under the receiver operating characteristic curve

<sup>a</sup> We oversampled the ERM class to balance the training dataset

As the society ages, idiopathic ERMs are expected to occur. In addition, as the number of cataract surgeries increases, the prevalence of secondary ERM also increase [32]. Compared to the high prevalence of ERM, attempts to screen for ERMs using CFP have been relatively insufficient. Using current deep learning systems that primarily target diabetic retinopathy, age-related macular degeneration, and glaucoma [33, 34], most patients with ERM encounter diagnostic delays during the screening stage. Permanent visual damage is possible if the ERM is left unattended because there are no symptoms in the early stages. Our work establishes a deep learning model that focuses on diagnosing ERM early and shows a higher performance than traditional data learning. Table 5 presents a literature review that investigates deep learning models for ERM detection using CFP. Previous studies have reported very high performance (ROC-AUCs > 0.95) in detecting membrane features using a large dataset from a single center [11, 35]. Deep learning using large-scale multicenter datasets has also achieved high diagnostic accuracy for ERM (ROC-AUCs > 0.99) [12].

However, obtaining large-scale pathological data from ERM is difficult. Therefore, methods for achieving high accuracy with limited pathological data should be further studied. To our knowledge, no previous study has investigated a deep learning model with StyleGAN2-based augmentation for ERM detection using CFP. If our proposed generative AI method continues to expand, we can create a deep-learning model that can accurately diagnose early ERMs.

Currently, the CFP is the standard image domain that dominates ophthalmic screening [37]. A deep learning-based diagnosis of OCT cross-sectional images was developed for ERM. However, the detection of ERM in CFP has been overlooked. In studies using OCT, deep learning models have shown very high accuracy in detecting ERM [6, 7, 38]. The OCT, however, captures the cross-section of several local areas of the retina, so it is difficult to scan all areas of the macula with it. Therefore, early ERM may be difficult to detect with OCT. alone. In contrast, the CFP is an imaging domain that briefly depicts the entire macula. A subtle difference

**Table 5** A literature review for deep learning studies for detecting epiretinal membrane in fundus photography images

Study (first author, year)	Dataset	AI architecture	Summary
Son, 2020 [11]	Local clinic data (ERM, 3639 eyes) + external database	Modified ResNet + classic augmentation	The deep learning model for retinal membrane feature detection showed ROC-AUCs of 0.989 and 0.997 in two validation sets
Casado-García, 2021 [31]	A nationwide database (Spain) + RFMID	HR-net + CycleGAN	The final model achieved a F1-score of 86.82% to detect ERM
Shao, 2021 [10]	Local clinic data (ERM, 83 eyes / no ERM, 61 eyes)	Inception-Resnet-v2 and Xception + classic augmentation	The AI model achieved an accuracy of 77.1%. It was comparable to manual reading (accuracy, 75.7%)
Kim, 2021 [36]	Local clinic data (ERM, 99 eyes / control, 79 eyes)	ResNet50 + classic augmentation	The deep learning model for ERM detection showed a sensitivity of 92.5% and specificity of 98.3%
Cen, 2021 [12]	JSIEC + LEDRS + EYEPAACS	Mask R-CNN + Inception-V3, Xception, InceptionResNet-V2, and modified ResNet and ResNeXt	The final model for ERM detection showed ROC-AUCs of 0.9972 and 0.9976 in two validation sets
Li, 2022 [13]	Local clinic data (ERM, 2947 eyes)	SeResNext50 + classic augmentation	The deep learning model for ERM detection showed ROC-AUCs of 0.968 in the internal validation and 0.938 and 0.934 in the external validation
Son, 2023 [35]	Local clinic data (ERM, 3073 eyes) + MESSIDOR	EfficientNet-B7 + classic augmentation	The deep learning model for membrane feature detection showed ROC-AUCs of 0.997 in the internal validation and 0.954 in the external validation
Ours	Local clinic data (ERM, 302 eyes / control, 1250 eyes) + RFMID + JSIEC	EfficientNetB0 + StyleGAN2	The proposed model achieved ROC-AUC of 0.926 for internal validation. ROC-AUCs of 0.951 and 0.914 were obtained for the two external validation datasets

ERM epiretinal membrane, EyePACS Eye Picture Archive Communication System Kaggle data, JSIEC Joint Shantou International Eye Center dataset, LEDRS Lifeline Express Diabetic Retinopathy Screening Systems, RFMID Retinal fundus multi-disease image dataset, ROC-AUC area under the receiver operating characteristic curve

between the cellophane reflex of the ERM and the normal reflection of the retina exists; distinguishing between them can be difficult for ophthalmologists. Timely surgical interventions can reduce the socioeconomic costs of late-stage ERM [39]. Therefore, developing and distributing a model that accurately screens ERM through continuous development is necessary.

We addressed the challenge of using an imbalanced dataset for ERM detection. Compared with conventional linear transformation augmentation (classic augmentation), GAN-based augmentation showed improved performance in the detection of ERM. In particular, the StyleGAN2 model generated relatively high-quality and realistic CFP images. This model performed better than the CNN models using DDPM-based or CutMix augmentation methods. ViT, which recently exhibited a higher performance than CNN architectures, failed to show a better performance than the proposed CNN model with StyleGAN2 augmentation. A previous study demonstrated that StyleGAN2 can synthesize mixed-style medical images by combining the features of the training sets [17]. To learn various samples and improve the generalization of deep learning models, StyleGAN2 could be adopted for out-of-distribution sample detection of computed tomography images [40]. Our study also confirms that StyleGAN2 is a promising generative AI technique for improving medical image synthesis and prediction performance. Generative AI continues to develop by adopting and expanding various numerical and probabilistic algorithms [14]. Recent advances in diffusion methods predict the future generation of higher-quality images [36]. A recent study showed that the diffusion model outperformed GAN techniques in the CFP, chest X-ray, and histopathology imaging domains [26]. There was an attempt to improve diagnostic performance in CFP by combining GAN and Transformer structures [41], and performance improvement is expected if applied to ERM in the future.

This study has several limitations. Firstly, we generated CFP images with relatively low resolution in the GAN models, which had a resolution of  $256 \times 256$  pixels. For the early diagnosis of ERM, it is necessary to analyze images with greater resolution. Secondly, the dataset included an East Asian population from a single healthcare center. Although the proposed model performed well on limited external validation datasets, models trained with data from a single institution are expected to degrade in performance in other clinical settings. Thirdly, the training and validation datasets included only a limited number of CFP images. Although GAN have been used to overcome the data shortage of ERM,

additional data collection is essential to achieve a higher performance.

## Conclusion

We propose an improved deep learning model by synthesizing realistic CFP images with the pathological features of ERM through generative AI. We leveraged a deep learning classification model with additional StyleGAN2 training to address limited data availability. The final model outperformed the typical augmentation and other GAN-based learning methods for detecting ERM using the CFP. We believe that our deep learning framework will help achieve a more accurate detection of ERM in a limited data setting.

## Abbreviations

AI	Artificial intelligence
AUC	Area under the receiver operating characteristics
CFP	Color fundus photography
CNN	Convolutional neural network
ERM	Epiretinal membrane
GAN	Generative adversarial network
JSIEC	Joint Shantou International Eye Center dataset
KNIBP	Korean National Institute for Bioethics Policy
RFMiD	Retinal fundus multi-disease image dataset
ROC	Receiver operating characteristics
OCT	Optical coherence tomography
SGD	Stochastic gradient descent

## Supplementary Information

The online version contains supplementary material available at <https://doi.org/10.1186/s12911-024-02431-4>.

**Additional file 1: Table S1.** Original code sources of GAN techniques.  
**Figure S2.** Sample anonymized color fundus photographs data with epiretinal membrane.

## Acknowledgements

None.

## Code availability

The original source codes of the GAN techniques are provided in the Supplementary Materials. In this study, we modified the source code to generate a CFP.

## Authors' contributions

JYC acquired and analyzed data, interpreted the results and drafted the manuscript. IHR, JKK, and ISL suggested the original study idea, interpreted the results, contributed to writing. TKY analyzed data and contributed to data interpretation and manuscript editing.

## Funding

None.

## Availability of data and materials

The healthcare center data used in this study cannot be made publicly accessible owing to KNIBP restrictions. Sample-anonymized CFP data with ERM are available in the Supplementary Materials. External databases included the retinal fundus multi-disease image dataset (RFMiD, available at <https://iee-dataport.org/open-access/retinal-fundus-multi-disease-image-dataset-rfmid>) [15] and the Joint Shantou International Eye Center dataset (JSIEC, available at <https://www.kaggle.com/datasets/linchundan/fundusimage1000>) [12].

## Declarations

### Ethics approval and consent to participate

This study was approved by the Institutional Review Board of the Korean National Institute for Bioethics Policy (KNIBP) and the need for informed consent from the patients was waived. All procedures were performed in accordance with the ethical standards of the institutional and national research committees and the 1964 Declaration of Helsinki and its later amendments or comparable ethical standards.

### Consent for publication

Not applicable.

### Competing interests

IHR and JKK are directors of VISUWORKS, and own company stock. IHR serves on the Advisory Board for Carl Zeiss Meditec AG and Avellino Lab USA/MAB for Avellino Lab Korea. TKY is an employee of VISUWORKS and received a salary or stock as part of the standard compensation package. The remaining authors declare no conflicts of interest.

Received: 29 July 2023 Accepted: 17 January 2024

Published online: 26 January 2024

## References

- Stevenson W, Prospero Ponce CM, Agarwal DR, Gelman R, Christoforidis JB. Epiretinal membrane: optical coherence tomography-based diagnosis and classification. *Clin Ophthalmol*. 2016;10:527–34.
- Kim JM, Lee H, Shin JP, Ahn J, Yoo JM, Song SJ, et al. Epiretinal Membrane: Prevalence and Risk Factors from the Korea National Health and Nutrition Examination Survey, 2008 through 2012. *Korean J Ophthalmol*. 2017;31:514–23.
- Kim JS, Kim M, Kim SW. Prevalence and risk factors of epiretinal membrane: Data from the Korea National Health and Nutrition Examination Survey VII (2017–2018). *Clin Experiment Ophthalmol*. 2022;50:1047–56.
- Far PM, Yeung SC, Ma PE, Hurley B, Kertes P, You Y, et al. Effects of Internal Limiting Membrane Peel for Idiopathic Epiretinal Membrane Surgery: A Systematic Review of Randomized Controlled Trials. *Am J Ophthalmol*. 2021;231:79–87.
- Fung AT, Galvin J, Tran T. Epiretinal membrane: A review. *Clin Experiment Ophthalmol*. 2021;49:289–308.
- Tang Y, Gao X, Wang W, Dan Y, Zhou L, Su S, et al. Automated Detection of Epiretinal Membranes in OCT Images Using Deep Learning. *Ophthalmic Res*. 2022;66:238–46.
- Sonobe T, Tabuchi H, Ohsugi H, Masumoto H, Ishitobi N, Morita S, et al. Comparison between support vector machine and deep learning, machine-learning technologies for detecting epiretinal membrane using 3D-OCT. *Int Ophthalmol*. 2019;39:1871–7.
- Cheung CY, Tang F, Ting DSW, Tan GSW, Wong TY. Artificial Intelligence in Diabetic Eye Disease Screening. *The Asia-Pacific Journal of Ophthalmology*. 2019;8:158.
- Cheng Y, Ma M, Li X, Zhou Y. Multi-label classification of fundus images based on graph convolutional network. *BMC Med Inform Decis Mak*. 2021;21:82.
- Shao E, Liu C, Wang L, Song D, Guo L, Yao X, et al. Artificial intelligence-based detection of epimacular membrane from color fundus photographs. *Sci Rep*. 2021;11:19291.
- Son J, Shin JY, Kim HD, Jung K-H, Park KH, Park SJ. Development and Validation of Deep Learning Models for Screening Multiple Abnormal Findings in Retinal Fundus Images. *Ophthalmology*. 2020;127:85–94.
- Cen L-P, Ji J, Lin J-W, Ju S-T, Lin H-J, Li T-P, et al. Automatic detection of 39 fundus diseases and conditions in retinal photographs using deep neural networks. *Nat Commun*. 2021;12:4828.
- Li B, Chen H, Zhang B, Yuan M, Jin X, Lei B, et al. Development and evaluation of a deep learning model for the detection of multiple fundus diseases based on colour fundus photography. *Br J Ophthalmol*. 2022;106:1079–86.
- You A, Kim JK, Ryu IH, Yoo TK. Application of generative adversarial networks (GAN) for ophthalmology image domains: a survey. *Eye and Vision*. 2022;9:6.
- Pachade S, Porwal P, Thulkar D, Kokare M, Deshmukh G, Sahasrabudhe V, et al. Retinal Fundus Multi-Disease Image Dataset (RFMiD): A Dataset for Multi-Disease Detection Research. *Data*. 2021;6:14.
- Iqbal T, Ali H. Generative Adversarial Network for Medical Images (MI-GAN). *J Med Syst*. 2018;42:231.
- Yoon D, Kong H-J, Kim BS, Cho WS, Lee JC, Cho M, et al. Colonoscopic image synthesis with generative adversarial network for enhanced detection of sessile serrated lesions using convolutional neural network. *Sci Rep*. 2022;12:261.
- Salehinejad H, Colak E, Dowdell T, Barfett J, Valae S. Synthesizing Chest X-Ray Pathology for Training Deep Convolutional Neural Networks. *IEEE Trans Med Imaging*. 2019;38:1197–206.
- Diaz-Pinto A, Colomer A, Naranjo V, Morales S, Xu Y, Frangi AF. Retinal Image Synthesis and Semi-Supervised Learning for Glaucoma Assessment. *IEEE Trans Med Imaging*. 2019;38:2211–8.
- Yoo TK, Choi JY, Kim HK. CycleGAN-based deep learning technique for artifact reduction in fundus photography. *Graefes Arch Clin Exp Ophthalmol*. 2020;258:1631–7.
- Karras T, Laine S, Aittala M, Hellsten J, Lehtinen J, Aila T. Analyzing and Improving the Image Quality of StyleGAN. *Proceedings of the IEEE/CVF Conference on Computer Vision and Pattern Recognition (CVPR)*. 2020:8110–9. <https://doi.org/10.1109/CVPR42600.2020.00813>.
- Huang J, Liao J, Kwong S. Unsupervised Image-to-Image Translation via Pre-Trained StyleGAN2 Network. *IEEE Trans Multimedia*. 2022;24:1435–48.
- Kim M, Kim YN, Jang M, Hwang J, Kim H-K, Yoon SC, et al. Synthesizing realistic high-resolution retina image by style-based generative adversarial network and its utilization. *Sci Rep*. 2022;12:17307.
- Ahn G, Choi BS, Ko S, Jo C, Han H-S, Lee MC, et al. High-resolution knee plain radiography image synthesis using style generative adversarial network adaptive discriminator augmentation. *J Orthop Res*. 2023;41:84–93.
- Shahzad A, Raza M, Shah JH, Sharif M, Nayak RS. Categorizing white blood cells by utilizing deep features of proposed 4B-AdditionNet-based CNN network with ant colony optimization. *Complex Intell Syst*. 2022;8:3143–59.
- Müller-Franzes G, Niehues JM, Khader F, Arasteh ST, Haaburger C, Kuhl C, et al. A multimodal comparison of latent denoising diffusion probabilistic models and generative adversarial networks for medical image synthesis. *Sci Rep*. 2023;13:12098.
- Kim HK, Ryu IH, Choi JY, Yoo TK. Early experience of adopting a generative diffusion model for the synthesis of fundus photograph. *Research square*, preprint, 2022. <https://doi.org/10.21203/rs.3.rs-2183608/v2>.
- Yun S, Han D, Chun S, Oh SJ, Yoo Y, Choe J. CutMix: Regularization Strategy to Train Strong Classifiers With Localizable Features. In: 2019 IEEE/CVF International Conference on Computer Vision (ICCV). 2019. p. 6022–31. <https://doi.org/10.1109/ICCV.2019.00612>.
- Gu Z, Li Y, Wang Z, Kan J, Shu J, Wang Q. Classification of Diabetic Retinopathy Severity in Fundus Images Using the Vision Transformer and Residual Attention. *Comput Intell Neurosci*. 2023;2023: e1305583.
- Kim KM, Heo T-Y, Kim A, Kim J, Han KJ, Yun J, et al. Development of a Fundus Image-Based Deep Learning Diagnostic Tool for Various Retinal Diseases. *J Pers Med*. 2021;11:321.
- Casado-García Á, García-Domínguez M, Heras J, Inés A, Royo D, Zapata MÁ, et al. Prediction of Epiretinal Membrane from Retinal Fundus Images Using Deep Learning. In: Alba E, Luque G, Chicano F, Cotta C, Camacho D, Ojeda-Aciego M, et al., editors. *Advances in Artificial Intelligence*. Cham: Springer International Publishing; 2021. p. 3–13.
- Kang KT, Kim KS, Kim YC. Surgical results of idiopathic and secondary epiretinal membrane. *Int Ophthalmol*. 2014;34:1227–32.
- González-Gonzalo C, Sánchez-Gutiérrez V, Hernández-Martínez P, Contreras I, Lechanteur YT, Domanian A, et al. Evaluation of a deep learning system for the joint automated detection of diabetic retinopathy and age-related macular degeneration. *Acta Ophthalmol*. 2020;98:368–77.
- Yoo TK. Actions are needed to develop artificial intelligence for glaucoma diagnosis and treatment. *J Med Artif Intell*. 2023;6:1–4.
- Son J, Shin JY, Kong ST, Park J, Kwon G, Kim HD, et al. An interpretable and interactive deep learning algorithm for a clinically applicable retinal fundus diagnosis system by modelling finding-disease relationship. *Sci Rep*. 2023;13:5934.

36. Pan S, Wang T, Qiu RLJ, Axente M, Chang C-W, Peng J, et al. 2D medical image synthesis using transformer-based denoising diffusion probabilistic model. *Phys Med Biol.* 2023;68: 105004.
37. Panwar N, Huang P, Lee J, Keane PA, Chuan TS, Richhariya A, et al. Fundus Photography in the 21st Century—A Review of Recent Technological Advances and Their Implications for Worldwide Healthcare. *Telemed J E Health.* 2016;22:198–208.
38. Jin K, Yan Y, Wang S, Yang C, Chen M, Liu X, et al. iERM: An Interpretable Deep Learning System to Classify Epiretinal Membrane for Different Optical Coherence Tomography Devices: A Multi-Center Analysis. *J Clin Med.* 2023;12:400.
39. Gupta OP, Brown GC, Brown MM. A Value-Based Medicine Cost-Utility Analysis of Idiopathic Epiretinal Membrane Surgery. *Am J Ophthalmol.* 2008;145:923-928.e1.
40. Woodland M, Wood J, Anderson BM, Kundu S, Lin E, Koay E, et al. Evaluating the Performance of StyleGAN2-ADA on Medical Images. In: Zhao C, Svoboda D, Wolterink JM, Escobar M, editors., et al., *Simulation and Synthesis in Medical Imaging.* Cham: Springer International Publishing; 2022. p. 142–53.
41. Yang Z, Zhang Y, Xu K, Sun J, Wu Y, Zhou M. DeepDrRVO: A GAN-auxiliary two-step masked transformer framework benefits early recognition and differential diagnosis of retinal vascular occlusion from color fundus photographs. *Comput Biol Med.* 2023;163: 107148.

### **Publisher's Note**

Springer Nature remains neutral with regard to jurisdictional claims in published maps and institutional affiliations.